Simulated niche partitioning by bacteria

Steven S. Andrews and Adam P. Arkin
Physical Biosciences Division
Lawrence Berkeley National Laboratory
1 Cyclotron Road
Berkeley, CA 94720
ssandrews@lbl.gov

1. Introduction

A central problem in ecology concerns the number of species that inhabit a given environment. A myriad of factors are involved, including speciation and extinction rates, geographic factors, seasonal cycles, food web stability, and a significant amount of random chance. The reductionist approach, taken here, is to reduce the system to its bare essentials and to then pose the question: is the biological community predictable for a simple given physical environment?

Our simplified system is a chemostat, which is a well stirred tank of bacterial growth medium that has been inoculated with a population of live bacteria. The culture is grown continually by adding fresh medium at a constant rate while simultaneously removing spent medium to maintain a constant volume. This model eliminates a tremendous amount of the complexity in natural environments: spatial issues are not relevant because the system is well mixed, diurnal and seasonal influences are removed, bacteria reproduce asexually so genetic recombination can be largely ignored, and an inoculating bacterial community can be selected in which there is no predation or parasitism. To simplify things even more, we investigate the chemostat model system with computer simulations so that every aspect is completely controlled and measurable. Clearly, the resulting toy system is no longer an accurate portrayal of natural ecology, although we believe that many of the essential factors are retained.

Continuous culture of bacteria often leads to competitive exclusion, meaning that one genotype outcompetes all others [1]. The resulting monoculture may evolve over time [2-4], sometimes with specific genomic changes that are the same in parallel experiments [5-7]. Evolution in a chemostat often proceeds with punctuated equilibria, in which periods of evolutionary stasis are periodically interrupted when faster growing mutants arise spontaneously and rapidly outcompete the resident population [8, 9]. A few experiments have also shown the stable coexistence of phenotypically distinct bacterial populations, a situation called niche partitioning [10, 11]. For example, a glucose limited continuous culture that was started with a single clone of *Escherichia coli* bacteria became polymorphic by generation number 773 with three populations that had different patterns of uptake and secretion of the metabolites acetate and glycerol [10].

Partly inspired by this experimental finding of coexistence, this work explores two simulated systems with niche partitioning, focusing on the steady-state result that is approached after many generations. We investigate ways in which the environment and the cellular design affect the co-existence of distinct populations.

2. Description of the model

The model system consists of a simulated chemostat populated with simulated bacteria. Bacterial growth dynamics are treated using a population balance method, in which the entire community of bacteria are subdivided into a collection of phenotypes. Within each phenotype, all individuals are completely identical, without individuality that could arise from cell age, history of the cell surroundings, or stochastics. As a typical chemostat experiment has a bacterial population with around 10^8 to 10^{11} individuals, this use of average bacterial properties is appropriate for a study of the long term behavior of a bacterial community. While it does not affect the results presented here, the population balance method is not always good for studies of dynamics; for example, it does not include the stochastic effects that lead to punctuated equilibria. An alternate method, called a cell ensemble method, simulates each bacterium individually so as to capture bacterial individuality, but at a high computational cost for large populations [12].

Simulated bacteria are defined with a few arrangements of a biochemical functional module (Figure 1). This module reduces a bacterial metabolic pathway to a sequence of simple chemical reactions for substrate import, metabolism, and export of product. This is, of course, a gross simplification of a highly complex and interconnected biological network. Import and export processes, which also account for diffusion to and from the cell surface, are treated using passive transport, leading to linear kinetics and reaction rate constants that are equal for both transport directions:

$$\begin{aligned} S \underset{k_x}{\overset{k_i}{\rightleftharpoons}} S' \qquad & \frac{dc_S}{dt} = k_i\left(c_S - c_S'\right) \\ P \underset{k_i}{\overset{k_x}{\rightleftharpoons}} P \qquad & \frac{dc_P}{dt} = k_x\left(c_P' - c_P\right) \end{aligned} \tag{1}$$

S denotes a substrate, P is a product, c_S and c_P are substrate and product concentrations in the bioreactor external to the cells, a prime symbol denotes chemicals or concentrations inside the cell, and k_i and k_x are import and export rate constants. Simplified metabolism is treated with a single-step conversion of substrate to product using Michaelis-Menten kinetics, which has the quasi-steady-state solution:

$$\begin{aligned} E + S \underset{k_r}{\overset{k_f}{\rightleftharpoons}} ES \overset{k_p}{\rightarrow} E + P \qquad & \frac{dc_P}{dt} = \frac{Vc_S}{K + c_S} \\ K = \frac{k_r + k_p}{k_f} \qquad & V = k_p\left[E_T\right] \end{aligned} \tag{2}$$

E denotes an enzyme, $[E_T]$ is the total concentration of the enzyme, k_f, k_r, and k_p are the forward, reverse, and product reaction rates respectively, K is the Michaelis-Menten constant, and V is the maximum reaction velocity (these latter symbols are typically shown as K_M and V_{max}, respectively, although the notation is abbreviated here to reduce clutter). Using these fundamental reactions for import, export, and metabolism, the quasi-steady-state solutions to the internal chemical concentrations were solved for the model metabolic networks, shown in Figure 1 as the column vector **c**'. While these solutions cannot capture transient behavior accurately, this work focuses on the long term behavior of the communities where they are appropriate.

The metabolic maximum reaction velocity V, or velocities V_1 and V_2, are essentially the only parameters that differentiate one phenotype from another within the networks. These parameters are allowed to evolve while the reaction rate constants are fixed, acting as biochemical constraints on evolution. In biological terms, we are assuming that the metabolic enzymes are constitutively expressed but that mutations can affect their expression levels, given by $[E_T]$. The

Network I

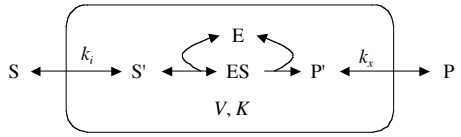

$$\mathbf{c} = \begin{bmatrix} c_S \\ c_P \end{bmatrix} = \begin{bmatrix} f_1(k_i, K, V, c_S) \\ \dfrac{Vc_S}{k_x(K + c_S)} + c_P \end{bmatrix}$$

$$\mathbf{u}(\mathbf{c}) = \begin{bmatrix} vk_i(c_S - c_S) \\ vk_x(c_P - c_P) \end{bmatrix} \qquad r(\mathbf{c}) = k_g\left[\boldsymbol{\nu}^T \cdot \mathbf{u}(\mathbf{c})\right]^{\gamma}(k_m + k_{m1}V)$$

Network II

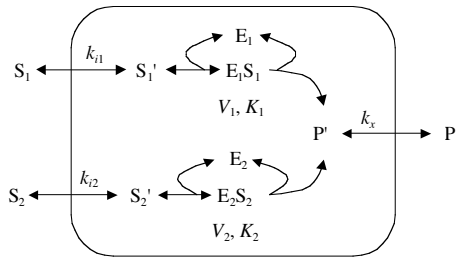

$$\mathbf{c} = \begin{bmatrix} c_{S1} \\ c_{S2} \\ c_P \end{bmatrix} = \begin{bmatrix} f_1(k_{i1}, K_1, V_1, c_{S1}) \\ f_1(k_{i2}, K_2, V_2, c_{S2}) \\ \dfrac{V_1 c_{S1}}{k_x(K_1 + c_{S1})} + \dfrac{V_2 c_{S2}}{k_x(K_2 + c_{S2})} + c_P \end{bmatrix}$$

$$\mathbf{u}(\mathbf{c}) = \begin{bmatrix} vk_{i1}(c_{S1} - c_{S1}) \\ vk_{i2}(c_{S2} - c_{S2}) \\ vk_x(c_P - c_P) \end{bmatrix} \qquad r(\mathbf{c}) = k_g\left[\boldsymbol{\nu}^T \cdot \mathbf{u}(\mathbf{c})\right]^{\gamma}(k_m + k_{m1}V_1 + k_{m2}V_2 + k_{m12}V_1V_2)$$

Network III

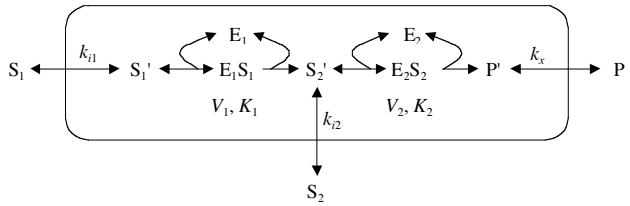

$$\mathbf{c} = \begin{bmatrix} f_1(k_{i1}, K_1, V_1, c_{S1}) \\ f_2(k_{i1}, K_1, V_1, c_{S1}, k_{i2}, K_2, V_2, c_{S2}) \\ \dfrac{V_2 c_{S2}}{k_x(K_2 + c_{S2})} + c_P \end{bmatrix}$$

$$\mathbf{u}(\mathbf{c}) = \begin{bmatrix} vk_{i1}(c_{S1} - c_{S1}) \\ vk_{i2}(c_{S2} - c_{S2}) \\ vk_x(c_P - c_P) \end{bmatrix} \qquad r(\mathbf{c}) = k_g\left[\boldsymbol{\nu}^T \cdot \mathbf{u}(\mathbf{c})\right]^{\gamma}(k_m + k_{m1}V_1 + k_{m2}V_2 + k_{m12}V_1V_2)$$

Required functions

$$f_1(k_i, K, V, c_S) \equiv \frac{1}{2k_i}\left[V + k_i c_S - k_i K + \sqrt{(V - k_i c_S + k_i K)^2 + 4k_i^2 K c_S}\right]$$

$$f_2(k_{i1}, K_1, V_1, c_{S1}, k_{i2}, K_2, V_2, c_{S2}) \equiv \frac{1}{2k_{i2}}\left[V_2 - f_1(k_{i1}, K_1, V_1, c_{S1}) - k_{i2}c_{S2} + k_{i2}K_2\right]$$
$$+ \frac{1}{2k_{i2}}\sqrt{\left(V_2 - f_1(k_{i1}, K_1, V_1, c_{S1}) - k_{i2}c_{S2} + k_{i2}K_2\right)^2 + 4k_{i2}K_2\left(k_{i2}c_{S2} + f_1(k_{i1}, K_1, V_1, c_{S1})\right)}$$

Figure 1. Biochemical networks and the corresponding equations for steady-state metabolism and growth. Variables that are not described in the text: v is the volume of a bacterium; k_m, k_{m1}, k_{m2}, and k_{m12} are Taylor series expansion coefficients for the maintenance energy; and $f_1(\ldots)$ and $f_2(\ldots)$ are steady-state solutions for c_S' in Network I and c_{S2}' in Network III, respectively.

one exception is that the import/export rate constant k_{i2} in Network III, described below and in Figure 1, is also a phenotypic parameter that is allowed to evolve. These parameters were chosen to represent the phenotype using the biological rationalization that enzyme expression levels are likely to evolve more quickly than enzyme kinetics. Also, preliminary simulations showed that if other parameters are allowed to evolve, they typically shift towards either the smallest or the largest values permitted, regardless of the chemical environment, leading to less interesting results.

The chemical environment of the medium is affected by: *i*) inflow to the chemostat and *ii*) nutrient uptake and waste excretion by bacteria:

$$\frac{\partial \mathbf{c}}{\partial t} = D\left(\mathbf{c}^{\dagger} - \mathbf{c}\right) - \sum_{p} X_p \mathbf{u}_p\left(\mathbf{c}\right) \tag{3}$$

$\mathbf{c}$ is the vector of chemical concentrations in the chemostat, $\mathbf{c}^{\dagger}$ is the chemical concentrations in the chemostat feed tube, D is the chemostat dilution rate, which is the ratio of the flow rate to the chemostat volume, X_p is the number density of bacteria with phenotype p, and $\mathbf{u}_p(\mathbf{c})$ is the uptake function which expresses the net rate of chemical uptake by a bacterium of phenotype p (Figure 1). Waste excretion is expressed with a negative uptake rate.

The other differential equation that defines the model quantifies the change of bacterial populations over time, where the processes are: *i*) loss of bacteria from the system due to chemostat flow, *ii*) net bacterial reproduction, and *iii*) transitions from one phenotype to another:

$$\frac{\partial X_p}{\partial t} = -DX_p + X_p r_p\left(\mathbf{c}\right) + \sum_{p'} \left(X_{p'} T_{pp'} - X_p T_{p'p}\right) \tag{4}$$

$r_p(\mathbf{c})$, called the growth function, is the net reproduction rate per individual of phenotype p, where this includes both cell division and natural cell death. $T_{pp'}$ is a matrix for the transition rate of phenotype p' to phenotype p. While this transition rate formalism could account for cell cycle effects, in which the phenotype changes over a cell's lifetime, it is assumed here that a cell's phenotype is invariant. This allows the matrix $T_{pp'}$ to be interpreted as the phenotype mutation rate, making the value of the summation term in eq. 4 much smaller than those of the first two terms, for most situations. For convenience, phenotype transitions are only permitted between neighboring phenotypes in the simulations, allowing the transition rate to be expressed as a diffusion coefficient.

The growth function used for the three networks is proportional to the free energy released by metabolism, less the maintenance energy of a cell:

$$r_p\left(\mathbf{c}\right) = k_g\left[\boldsymbol{\mu}'^{\mathrm{T}} \cdot \mathbf{u}\left(\mathbf{c}\right) - k_{m,p}\right] \tag{5}$$

k_g is the cell yield for a unit amount of available energy, $\boldsymbol{\mu}'$ is a column vector of chemical potentials inside the cell, $\boldsymbol{\mu}'^{\mathrm{T}}$ is its transpose, and $k_{m,p}$ is the maintenance energy for phenotype p. Following the usual definition [13] and assuming ideal solutions, the chemical potential of species i is

$$\mu_i = \mu_i^\circ + RT \ln \frac{c_i}{c_i^\circ} \tag{6}$$

μ_i° is the standard chemical potential of chemical i at the standard concentration c_i°, and RT is the thermodynamic temperature. The former term of eq. 6 represents both the enthalpy and the entropy of the chemical at the standard concentration while the latter term represents the entropic change that arises from a change in the concentration. As shown in Figure 1, the maintenance energies are treated using a simple Taylor series expansion of the function $k_{m,p}$ in terms of the phenotype parameters, which is truncated after the linear terms. The constant term of the series represents the maintenance energy for all cell processes except metabolism, terms proportional to V, V_1, or V_2 represent the energy used to synthesize the respective metabolic enzymes, and terms proportional to V_1V_2 represent interactions between metabolic pathways. Interactions can arise biologically from the sharing of enzymes by multiple pathways or the cross-inhibition of separate pathways.

There are several reasons for choosing these uptake and growth functions rather than one of the commonly used empirical functions [14, 15]. They are based on a physical model, allowing a direct and intuitive correspondence between mathematical parameters and physical properties. Also, they obey all physical constraints including mass conservation of chemicals and a free energy decrease for forward reactions (assuming a positive maintenance energy). With certain parameter choices, the Network I equations can be simplified to either the Monod or the Westerhoff growth function, which have been shown to accurately represent biological data [15, 16]. Finally, as shown below, these models produce interesting results because the metabolic maximum reaction velocities evolve toward finite values, rather than toward the ends of permitted parameter ranges. However, the parameter choices that are required to make this last point true are different from those that make the equations agree with experimental data on bacterial growth rates [15]. Differences arise primarily from the inability of these simulated bacteria to adapt to varying nutrient concentrations. Because of the discrepancy, quantitative values are only given for Network I and they are presented to give a sense of scale, rather than as biological predictions.

3. Results

3.1 Network I

The first network is composed of a single metabolic module that simply converts substrate to product. It was chosen to demonstrate the basic results of our uptake and growth functions in the population balance method, as well as simple evolution. It also forms a basis for comparison, both with Networks II and III which reduce to Network I in certain limits, and with experimental data [14-16].

The temporal growth dynamics of Network I are best illustrated with simulated batch growth, in which the growth medium is relatively rich at the beginning and is not refreshed (Figure 2A). Following the standard pattern, the bacterial population size grows exponentially until the nutrients are largely depleted, it levels off to form a stationary phase, and then it decreases during a long so-called death phase due to starvation. The stationary phase in the simulation is relatively short when compared to experimental results because these simulated bacteria have a maintenance energy cost that is independent of the environment, whereas real bacteria can adapt to low nutrient conditions.

Continuous growth is investigated by allowing a population to equilibrate in a chemostat at each of several dilution rates (Figure 2B), recording the population density and chemical

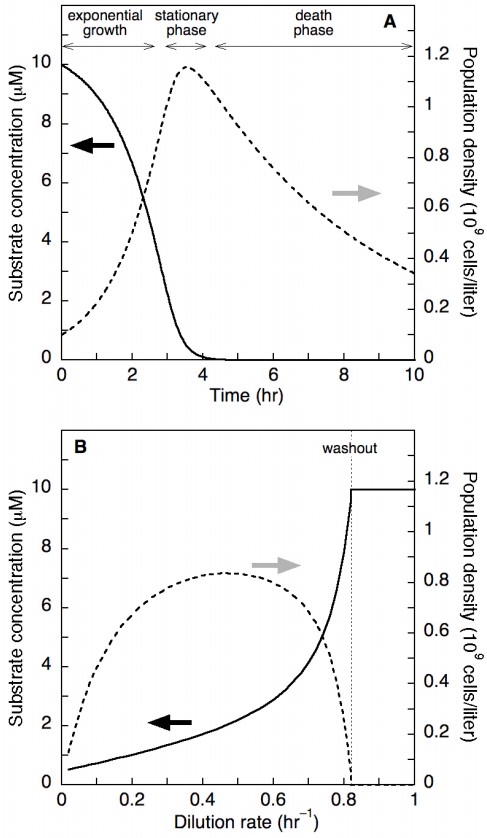

Figure 2. Simulated bacterial growth dynamics for Network I over time during batch growth (A) and at steady-state as a function of the dilution rate (B). Solid lines show the concentration of substrate (left axis) and dashed lines show the bacterial population density (right axis). Parameters: $k_i = k_x = 1000$ s^{-1}, $K = 0.5$ μM, $k_g = 5 \times 10^7$ cells/J, $k_{m1} = 5 \times 10^{-16}$ J μM^{-1} cell^{-1}, $k_m = 10^{-13}$ J s^{-1} cell^{-1}, $RT = 0.0026$ J/μmol, $V = 2000$ μM s^{-1}, $v = 10^{-6}$ l, $\mu_S^\circ = 3$ J μmol^{-1}, and $\mu_P^\circ = 0$. For (A), $c_S(0) = 10$ μM, $c_P(0) = 0$, and $X(0) = 10^{-8}$ cells. For (B), $c_S^\dagger = 10$ μM and $c_P^\dagger = 0$.

concentrations at each steady state. At steady-state and with a negligible mutation rate, eq. 4 has two solutions:

$$\begin{aligned} r_p(\mathbf{c}) &= D \\ X_p &= 0 \end{aligned} \tag{7}$$

The former solution applies to the portion of Figure 2B where the dilution rate is less than about 0.82 hr^{-1}; since the dilution rate is equal to the growth rate, the solid line in the figure also relates the growth rate to the substrate concentration. The simulation result was confirmed to be identical to the analytical result given in Figure 1. When the dilution rate exceeds the bacterial growth rate at the feed chemical concentrations, the bacteria cannot grow fast enough to replace those that are washed out of the system, leading to a state called washout in which the latter

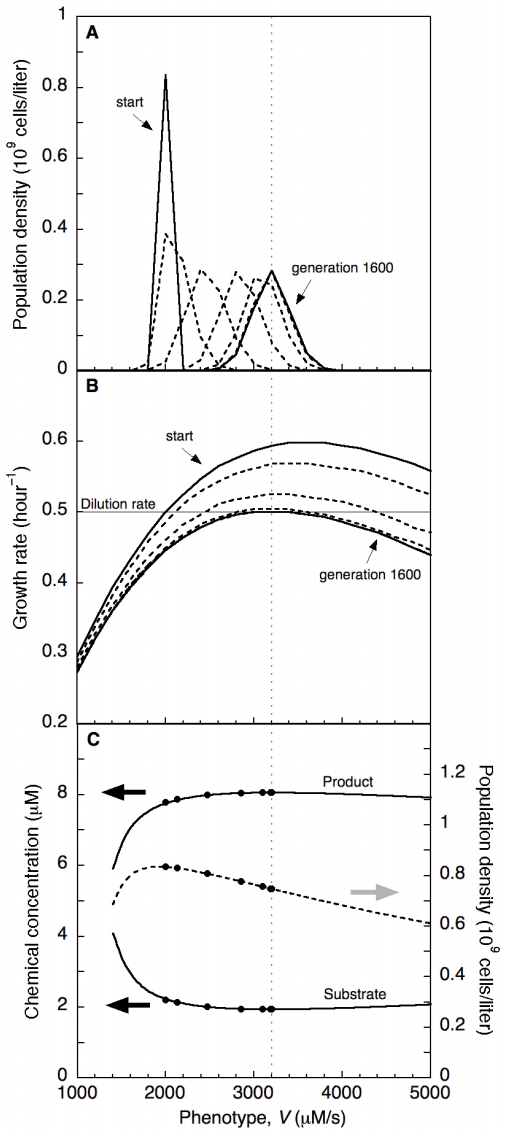

Figure 3. Evolutionary dynamics for Network I over 1600 generations. (A) Population density as a function of the phenotype, where the phenotype is classified into 200 μM/s wide bins. Curves are shown for generation 0 (solid line), 50, 100, 200, 400, 800, and 1600 (solid line). (B) Growth functions for the same time points. (C) Chemical concentrations and total population density for the same time points (dots) shown on lines generated with equivalent simulations that started with V=1400 μM/s or 5000 μM/s. Parameters are the same as in Figure 2, with the following additions: $D = 0.5$ hr^{-1}, phenotype diffusion rate = 0.02 μM^2 s^{-3}.

solution of eq. 7 applies. These simulated curves are in qualitative agreement with experimental results [14].

When the bacterial phenotype that was used to generate Figure 2 is left in a chemostat for many generations, the metabolic maximum reaction velocity, V, evolves to a larger value (Figure 3A). The numerical procedure is that 21 phenotypes were defined with V values ranging from 1000 to 5000 μM/s. The virtual chemostat was inoculated with cells with phenotype V = 1400

□M/s, the mutation rate was set to zero until the population size and extracellular chemical concentrations had stabilized (curves marked "start" in Figure 3), and then mutations were allowed again while the results shown in the figure were recorded. Because mutation is only possible between neighboring phenotypes, it is quantified with a diffusion coefficient, listed in the Figure 2 caption. This evolution can be understood by considering the growth rate as a function of the phenotype (Figure 3B). In Figure 3B, the initial population is localized to the intersection of the growth rate function and the horizontal line that marks the dilution rate (eq. 7). Mutational diffusion leads to populations with larger and smaller phenotype values; those with larger values are seen to have a faster growth rate than the others, so they multiply, take up more nutrient and thereby decrease the growth rate for all phenotypes, and the other bacteria starve. This process leads to an evolutionary drift of the phenotype that continues until no other phenotype has a faster growth rate. In the language of evolutionary game theory, the resulting phenotype is an evolutionarily stable strategy because the culture cannot be invaded by any other phenotype [17].

The same optimization is shown in a different way in Figure 3C. Here, it is seen that evolution results in the phenotype that minimizes the concentration of substrate in the medium and maximizes the concentration of waste (because of the stoichiometry of Network I, these are dependent parameters). However, evolution neither maximizes nor minimizes the population density. The lines in Figure 3C were produced with evolution simulations that are identical to the one shown in panels A and B, but starting with V = 1400 □M/s or V = 5000 □M/s. In both cases, evolution resulted in phenotypic drift towards the vertical line shown in the figure at V = 3204 □M/s.

Another phenomenon seen in Figure 3A is the spreading of the population distribution from the initial monoculture to a broader profile. This arises from a combination of mutational diffusion away from the center of the peak and a constant loss of the slower growing phenotypes at the edges of the distribution due to their slower growth rates.

3.2 Network II

The situation is more interesting with Network II, which has two parallel metabolic modules that consume different substrates from the medium but excrete the same waste product. In the simulation, the two substrates are added to the medium at the same rate, but are assigned slightly different standard chemical potentials to avoid artifacts that might arise with a perfectly symmetric system. This network represents real bacteria that are grown with multiple nutrients where it is found that all substrates are consumed simultaneously [18]. However, it is not clear if every bacterium consumes all substrates or if the population becomes phenotypically heterogeneous with different individuals specializing on different substrates.

The evolutionary dynamics of this network were found to be similar to those of Network I in that evolution proceeds with a monotonic phenotypic drift towards a steady-state population distribution (data not shown). These final distributions were recorded as a function of the chemostat dilution rate (Figure 4), using dilution rates that were increased in steps that were separated by long delays to allow the population to achieve steady-state before continuing. At low dilution rates, the bacterial community spontaneously partitions itself into two stable co-existing phenotypes, each of which specializes on metabolism of one of the two nutrients (Figure 4A). At higher dilution rates, there is a rapid transition from a pair of specialist phenotypes to a single generalist phenotype that metabolizes both nutrients (Figures 4C and D). At the transition (Figure 4B), there is a range of dilution rates about 0.03 units wide where there are three co-existing populations, including both specialist phenotypes and the generalist phenotype.

Using a dilution rate that is decreased rather than increased, exactly the same simulation results are found except quite close to the transition, which is shifted by about 0.07 units towards a lower dilution rate, indicating the presence of hysteresis. This niche partitioning bistability occurs despite the fact that every steady-state population was confirmed to be an evolutionarily stable strategy (for all phenotypes p, either $r_p(\mathbf{c}) < D$ or $X_p > 0$). It has not been investigated analytically.

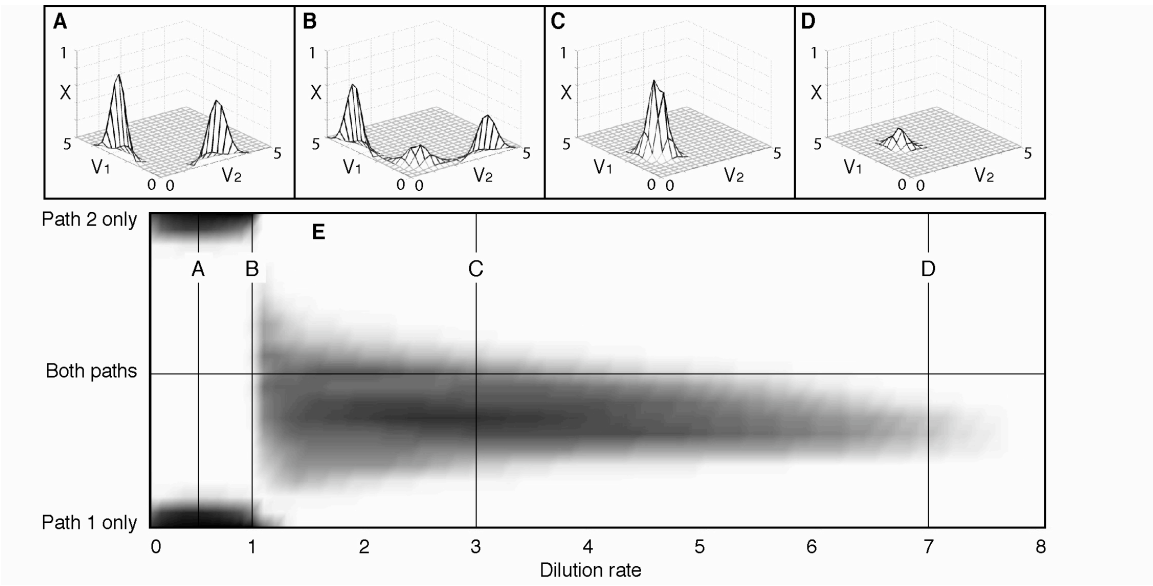

Figure 4. Steady-state population distributions across phenotypes for Network II as a function of the dilution rate. (A-D) Population densities in terms of the two phenotype parameters showing (A) stable coexisting specialist populations, (B) specialist and generalist populations, and (C and D) a single generalist population. (E) Population distribution as a function of the dilution rate, where dark regions represent high population density and light regions represent low population density. The vertical axis corresponds linearly to the angle between the phenotype parameters V_1 and V_2 so that specialist populations appear at the top and bottom of the panel and generalist populations appear in the middle. The dilution rates at which panels (A-D) were recorded are shown with vertical lines. Washout occurred at $D = 8.0$. Parameters: $k_{i1} = k_{i2} = k_x = 1.0$, $K_1 = K_2 = 1.0$, $k_g = 1.0$, $RT = 0.1$, $k_m = 0.1$, $k_{m1} = k_{m2} = 0.1$, $k_{m12} = 0.5$, $c_{S1}^{\dagger} = c_{S2}^{\dagger} = 1.0$, $c_P^{\dagger} = 0$, $\square_{S1}^{\circ} = 10.0$, $\square_{S2}^{\circ} = 8.0$, $\square_P^{\circ} = 0$, and mutational diffusion coefficients of 0.001 on each axis.

The pathway interaction term in the Network II maintenance energy expansion given with the constant k_{m12} is responsible for the niche partitioning found at low dilution rates. A positive value of k_{m12} promotes specialization because it imposes an energetic cost on bacteria that express both metabolic enzymes, in addition to the costs for each enzyme separately. With low dilution rates, substrate concentrations are low, so the available metabolic energy is low, and k_{m12} is large enough to promote specialization. In contrast, the interaction cost is smaller relative to the metabolic energy at higher dilution rates, thus lessening its influence and promoting generalization.

The relationship between the two specialist populations at low dilution rates is expressed with the community matrix, **A**, which quantifies the influence of a change of one population size on the growth rate of another population [19]. In this model system, populations only interact via extracellular chemical concentrations, so perturbing one population size does not have an immediate effect on other populations. Instead, the effect is directly proportional to the duration of the perturbation:

$$A_{pp\square} \equiv \frac{\partial \dot{X}_p}{\partial X_{p\square}} = X_p \frac{\partial r_p(\mathbf{c})}{\partial X_{p\square}} = X_p \square_{\mathbf{c}} r_p(\mathbf{c}) \cdot \frac{\partial \mathbf{c}}{\partial X_{p\square}} = X_p \square_{\mathbf{c}} r_p(\mathbf{c}) \cdot \frac{\partial \dot{\mathbf{c}}}{\partial X_{p\square}} dt$$
$$= \square X_p \square_{\mathbf{c}} r_p(\mathbf{c}) \cdot \mathbf{u}_{p\square}(\mathbf{c}) \square t \tag{8}$$

$A_{pp'}$ is the element of the community matrix for the effect of phenotype p' on phenotype p. The matrix for the specialist populations shown in Figure 4A was calculated using eq. 8, where the values of X_p and **c** were taken from the simulation results and numerical derivatives were taken of the growth function. Considering just the two most populated phenotypes, the matrix is:

$$\mathbf{A} = \begin{bmatrix} -0.588 & 0.0006 \\ 0.0004 & -0.437 \end{bmatrix} t \tag{9}$$

The first row and column are for the population that expresses pathway 1 and the second row and column are for the population that expresses pathway 2. The negative values on the main diagonal of **A** imply that population growth rates decrease when the population size is made larger than the steady-state value and vice versa, leading to negative feedback. The small negative values on the off-diagonal imply that the two populations are in weak competition with each other [19]. In this case, they are not competing for nutrients, but for the ability to get rid of waste products where the product inhibition on the growth rate arises from eq. 6. The eigenvalues of eq. 9 are very nearly the same as the diagonal terms; their negative values confirm that the community of specialist populations is stable to population size fluctuations [19].

3.3 Network III

In the third network, the metabolic modules are arranged sequentially rather than in parallel (Figure 1), such that a bacterium could metabolize S_1 to S_2, S_1 to P, or S_2 to P, where S_1 is a high energy nutrient and S_2 is a low energy nutrient. For simplicity, we return to adding only a single substrate to the chemostat (negligible amounts of S_2 and P are also added to avoid numerical errors arising from the logarithmic term in eq. 6). The rate constant for the import or export of the intermediate metabolite is made a third evolvable parameter to allow a wider range of phenotypes although it does not contribute to the maintenance energy. This network represents *Escherichia coli* bacteria grown on glucose, which can export or import the intermediate metabolites glycerol and acetate [10]. It also represents the yeast *Saccharomyces cerivisiae*, which can ferment glucose to ethanol to release a small amount of energy or respire glucose to carbon dioxide and water to release much more energy [20].

Niche partitioning with Network III is similar to that found for Network II, with the bacterial community composed of two specialist populations at low dilution rates and a single population at high dilution rates (Figure 5). While not shown in the figure, the original data show that the value of k_{i2} evolves to its maximal value for both specialist populations, implying that one population metabolizes substrate S_1 to S_2 and exports S_2, while the other population imports S_2 and metabolizes it to product. At high dilution rates, k_{i2} evolves to its minimal value. Here, the single population metabolizes S_1 fully to product without letting the S_2 intermediate escape to the surroundings. When the dilution rate dependence is simulated using decreasing flow rates, the transition from a single population to two populations occurs within 0.1 units as it does for increasing rates, indicating minimal or no bistability.

The transition from specialist populations to a single population occurs for a similar reason as for Network II. At low nutrient levels, the pathway interaction cost is sufficiently large compared to available energy that bacteria grow faster if they just metabolize S_1 to S_2, rather than metabolizing it all the way to product. This opens up a niche for a second specialist phenotype which metabolizes S_2 to product. At high dilution rates, the pathway interaction cost is minimal compared to the cost of losing S_2 to the environment, so cells grow faster if they include both metabolic modules and shut off S_2 transport.

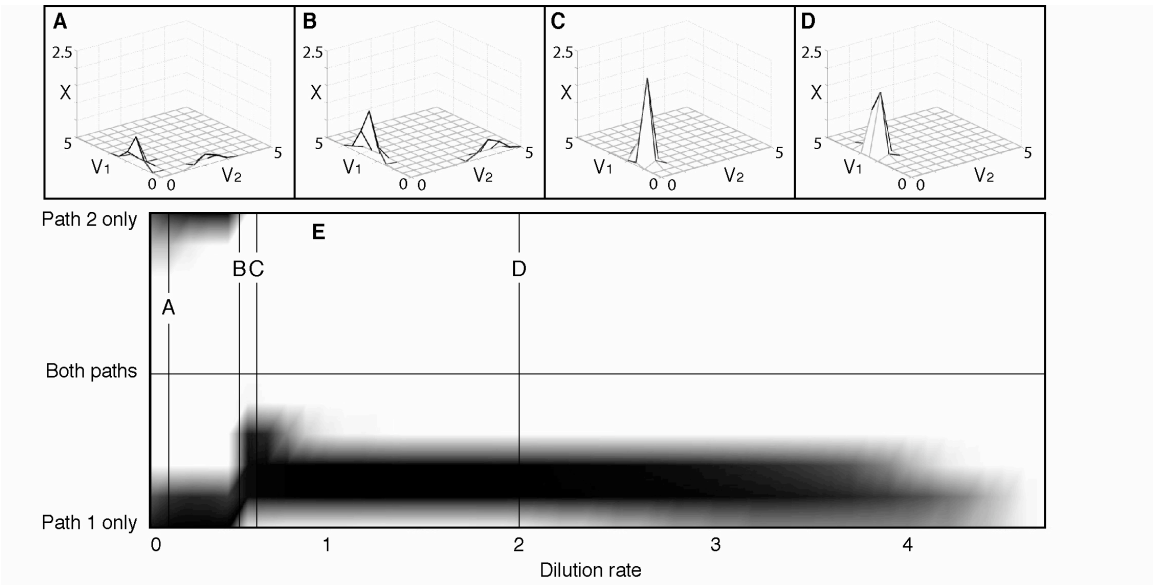

Figure 5. Steady-state population distributions across phenotypes for Network III as a function of the dilution rate. See the caption for Figure 4. The specialist populations shown in panels (A) and (B) evolved to have a value of k_{i2} equal to 2, which is the maximum permitted, while the generalist populations shown in panels (C) and (D) have a k_{i2} value equal to 0.01, which is the minimum value allowed. Washout occurred at $D = 4.9$. Parameters are the same as for Figure 4, except for k_{i2} which is an evolvable parameter here and the following: $c_{S1}^{\dagger} = 0.98$, $c_{S2}^{\dagger} = c_P^{\dagger} = 0.01$, and $\square_{S2}^{\circ} = 4.0$.

The community matrix for the specialist populations shown in Figure 5A is

$$\mathbf{A} = \begin{bmatrix} -0.0644 & 0.0015 \\ 0.0677 & -0.1282 \end{bmatrix} t \tag{10}$$

As before, the first row and column are for the "path 1 population" and the second row and column are for the "path 2 population". The negative values on the main diagonal again indicate that each population is independently stable. However, the positive values on the off-diagonal show that these populations are mutualistic rather than competitive [19]. The benefit of the path 1 population on the path 2 population, quantified with the value in the lower left corner of **A**, arises from the reliance of the latter phenotype on the metabolic product of the former phenotype. The metabolic energy available to the path 1 population is larger when the path 2 population reduces the concentration of S_2 in the medium, providing the much smaller benefit quantified in the upper right corner of **A**. The eigenvalues of the matrix are –0.063 and –0.130, indicating that this bacterial community is stable to population size fluctuations.

4. Discussion and conclusions

The model networks examined here are quite simple but are rich enough to yield interesting behaviors, including evolutionary optimization and niche partitioning that is dependent on the chemostat dilution rate. While minimal use was made of it in this work, the fact that the networks are based on the laws of thermodynamics rather than empirical observations is appealing. Because of it, one has a greater freedom in exploring parameter space and there is no fundamental reason

why behaviors found with these networks, or with any of a wide variety of similar models, could not be found with biological experiments.

Using Network I, the maximum metabolic reaction velocity was found to evolve to a final value in which the growth function is equal to the dilution rate for this phenotype, and has a lower value for all other phenotypes. This allows it to be identified as an evolutionarily stable strategy. This final phenotype is also the one that minimizes the substrate concentration in the chemostat and maximizes the product concentration. Assuming that the growth function is suitably well-behaved, the latter result can be derived from the former. Labeling the stable phenotype as p^*, the derivative of the steady-state chemical concentrations with respect to the phenotype at p^* is:

$$\left.\frac{d\mathbf{c}}{dp}\right|_{p^*} = \frac{\partial \mathbf{c}}{\partial r_p(\mathbf{c})} \left.\frac{\partial r_p(\mathbf{c})}{\partial p}\right|_{p^*} = 0 \tag{11}$$

The second equality follows from the fact that the latter partial derivative is zero, because the growth rate is maximal at p^* (see Figure 3). Similarly, the negative curvature of $r_p(\mathbf{c})$ at p^* can be used to show that evolution proceeds to minimize the substrate concentration while maximizing the product concentration, as was found in the simulations and is observed experimentally [8]. The result in eq. 11 can be readily generalized to all systems that obey the basic population balance model that was defined by eqs. 3 and 4, including those with multiple stable coexisting phenotypes (assuming there is a single steady-state and that functions are reasonably well-behaved). Since the chemical concentrations in the medium are stationary with respect to the phenotype at the evolutionary end-point, any thermodynamic function that depends on just these concentrations must also be stationary. It is likely that an optimizing function could be found for Networks II and III that is analogous to the substrate minimization that was found for Network I.

Both Networks II and III show coexistence at low dilution rates and single populations at high rates. Coexistence is not a necessary consequence of low dilution rates, which was confirmed by running simulations with decreased values of the interaction term in the maintenance energy, k_{m12}. This moves the transition between one and two populations to a lower dilution rate, eventually reaching zero, so that it becomes impossible to achieve coexistence. In contrast, there are never coexisting populations at chemostat washout, except in cases of perfect symmetry in the growth equation or growth rates that are identical by coincidence. As washout is approached, the medium chemical concentrations approach the feed concentrations, $\mathbf{c}^\dagger$. Because coexisting populations in this model only interact with each other via chemical concentrations, these interactions are reduced to zero at washout. Meanwhile, the growth function becomes $r_p(\mathbf{c}^\dagger)$, which is likely to be maximal for only a single phenotype. This maximum value is the washout dilution rate and the phenotype where it is maximum is the sole population that exists just before washout.

These results suggest various experiments. In particular, bacterial evolution has been observed using continuous culture, resulting in either a single population or coexisting populations. If the dilution rates were varied, would it be possible to experimentally vary the degree of niche partitioning? Our results indicate that the answer is yes.

Acknowledgements

This work was funded by a postdoctoral research fellowship in Informational Biosciences from the National Science Foundation awarded to SSA, by the Lawrence Berkeley National Laboratory, and the United States Department of Energy. SSA would like to thank Chris Clark and Michelle Minikel for helpful discussions.

References

[1] Smith, H.L. and P. Waltman, *The theory of the chemostat, Dynamics of microbial competition*. Cambridge Univ. Press Cambridge (1995).

[2] Elena, S.F. and R.E. Lenski, "Evolution experiments with microorganisms: the dynamics and genetic bases of adaptation" *Nat. Rev. Genet.*, **4** (2003), 457-469.

[3] Velicer, G.J. and K.L. Stredwick, "Experimental social evolution with *Myxococcus xanthus*" *Antonie van Leeuwenhoek*, **81** (2002), 155-164.

[4] Bohannan, B.J.M. and R.E. Lenski, "Linking genetic change to community evolution: insights from studies of bacteria and bacteriophage" *Ecology Lett.*, **3** (2000), 362-377.

[5] Ferea, T.L., et al., "Systematic changes in gene expression patters following adaptive evolution in yeast" *Proc. Natl. Acad. Sci. USA*, **96** (1999), 9721-9726.

[6] Dunham, M.J., et al., "Characteristic genome rearrangements in experimental evolution of *Saccharomyces cerevisiae*" *Proc. Natl. Acad. Sci. USA*, **99** (2002), 16144-16149.

[7] Cooper, T.F., D.E. Rozen, and R.E. Lenski, "Parallel changes in gene expression after 20,000 generations of evolution in *Escherichia coli*" *Proc. Natl. Acad. Sci. USA*, **100** (2003), 1072-1077.

[8] Wick, L.M., H. Weilenmann, and T. Egli, "The apparent clock-like evolution of *Escherichia coli* in glucose-limited chemostats is reproducible at large but not at small population sizes and can be explained with Monod kinetics" *Microbiol.*, **148** (2002), 2889-2902.

[9] Lenski, R.E. and M. Travisano, "Dynamics of adaptation and diversification: A 10,000-generation experiment with bacterial populations" *Proc. Natl. Acad. Sci. USA*, **91** (1994), 6808-6814.

[10] Rosenzweig, R.F., et al., "Microbial evolution in a simple unstructured environment: genetic differentiation in *Escherichia coli*" *Genetics*, **137** (1994), 903-917.

[11] Notley-McRobb, L. and T. Ferenci, "The generation of multiple co-existing *mal*-regulatory mutations through polygenic evolution in glucose-limited populations of *Escherichia coli*" *Environ. Microbiol.*, **1** (1999), 45-52.

[12] Henson, M.A., "Dynamic modeling of microbial cell populations" *Curr. Opin. Biotechnol.*, **14** (2003), 460-467.

[13] Atkins, P.W., *Physical Chemistry*. third ed. W.H. Freeman and Co. New York (1986).

[14] Bailey, J.E. and D.F. Ollis, *Biochemical Engineering Fundamentals*. Second ed. McGraw Hill New York (1986).

[15] Senn, H., et al., "The growth of *Escherichia coli* in glucose-limited chemostat cultures: a re-examination of the kinetics" *Biochim. Biophys. Acta*, **1201** (1994), 424-436.

[16] Lendenmann, U., M. Snozzi, and T. Egli, "Growth kinetics of *Escherichia coli* with galactose and several other sugars in carbon-limited chemostat culture" *Can. J. Microbiol.*, **46** (2000), 72-80.

[17] Smith, J.M., *Evolution and the Theory of Games*. Cambridge University Press Cambridge (1982).

[18] Lendenmann, U., M. Snozzi, and T. Egli, "Kinetics of the simultaneous utilization of sugar mixtures by *Escherichia coli* in continuous culture" *Appl. Environ. Microbiol.*, **62** (1996), 1493-1499.

[19] May, R.M., *Stability and Complexity in Model Ecosystems*. 2nd ed. Princeton University Press Princeton (1974).

[20] Frick, T. and S. Schuster, "An example of the prisoner's dilemma in biochemistry" *Naturwissenschaften*, **90** (2003), 327-331.